Thermally deactivated energy transfer in Bi^{3+}-Yb^{3+} codoped Y_2O_3:
Evidence for the exchange interaction mechanism

Ting Yu,[1,2] Dechao Yu,[2] Qinyuan Zhang,[1,*] and Andries Meijerink[2,*]

[1]*State Key Laboratory of Luminescent Materials and Devices, and Institute of Optical Communication Materials,*
South China University of Technology, Guangzhou 510641, People's Republic of China
[2]*Condensed Matter and Interfaces, Debye Institute for Nanomaterials Science, Utrecht University,*
Princetonplein 5, 3584 CC Utrecht, The Netherlands

Y_2O_3 codoped with Bi^{3+} and Yb^{3+} is considered as an efficient downconversion material combining strong broadband absorption of Bi^{3+} with photon splitting by cooperative energy transfer from Bi^{3+} to two Yb^{3+} neighbors. However, evidence for photon splitting is lacking. Here we investigate the Bi^{3+}-to-Yb^{3+} energy-transfer mechanism. For cooperative energy transfer the Yb^{3+}-concentration-dependent luminescence decay will show clear characteristics of cooperative dipole-dipole transfer. Analysis of Yb^{3+}-concentration and temperature-dependent decay curves however demonstrates that the energy-transfer mechanism is not cooperative but single step, probably through a Bi^{4+}-Yb^{2+} charge-transfer state. The temperature dependence of the Bi^{3+}-to-Yb^{3+} energy-transfer efficiency is unusual as it decreases with temperature, unlike commonly observed thermally activated energy transfer. This is a signature of energy transfer via exchange interaction. The present results provide evidence for the absence of photon splitting in $Y_2O_3 : Bi^{3+}$, Yb^{3+} and form a convincing demonstration of exchange interaction mediated energy transfer.

I. INTRODUCTION

Downconversion (also known as quantum cutting or quantum splitting) involves conversion of one high-energy photon into two or more lower-energy photons [1,2]. Efficient downconversion materials are of great interest for application in solar cells [3–8], lighting, and displays [9–13]. Lanthanide ions are suitable candidates for downconversion because they have a rich energy-level structure with discrete energy levels that offer a wide variety of options for downconversion in different spectral regions [14–17]. For downconversion for photovoltaics, the Yb^{3+} ion is an attractive candidate as it has only two energy levels, a $^2F_{7/2}$ ground state and a $^2F_{5/2}$ excited state around $10\,000\,cm^{-1}$. The near-infrared (NIR) emission of Yb^{3+} is just above the band gap of c-Si solar cell (about 1.12 eV, 1100 nm), and thus it can serve as acceptor and emitter in downconversion materials [18–20]. A variety of downconversion lanthanide couples has been reported based on using Yb^{3+} as acceptor and Pr^{3+}, Tm^{3+}, Tb^{3+}, Nd^{3+}, and Ho^{3+} as donor ions [21–29]. Due to the weak absorption cross sections and narrow absorption linewidths of lanthanide ion donors, only a small fraction of solar spectral range can be utilized, limiting the practical application in solar cells.

To realize efficiently absorbing downconversion materials a sensitizer or efficient broadband-absorbing donor ion is required. As a potential candidate considerable attention has been focused on the s^2 ion Bi^{3+}, featuring the relatively strong and broadband absorption in ultraviolet (UV) to blue region [30–32]. More recently, efficient downconversion via cooperative energy-transfer (ET) mechanism has been reported in a variety of materials codoped with Bi^{3+} and Yb^{3+} [33–35]. However, evidence for a downconversion mechanism and photon splitting are lacking. It is challenging to distinguish between one-to-one and one-to-two photon conversion as in both cases a high-energy photon is converted into a lower-energy photon. Based on the experimental results that show efficient Bi^{3+} to Yb^{3+} ET already at low Yb-doping levels and the typical radiative rate of Bi^{3+} at room temperature ($\sim 10^7\,s^{-1}$) [30,31], compared to the cooperative transfer rate ($\sim 10^3\,s^{-1}$ for Tb^{3+}-Yb^{3+} in YPO_4) [21], there is doubt about the cooperative ET mechanism for the (Bi^{3+}, Yb^{3+}) couple.

One way to obtain evidence for a cooperative ET mechanism is to model the donor emission decay curves for different acceptor (here Yb^{3+}) concentrations [21,25,26,36,37]. For cooperative dipole-dipole interaction the rate of ET is proportional to the inverse sixth power of the donor-acceptor distance for both acceptors [21,37–40]. The transfer efficiency is independent of the lifetime of excited state on the donor as both the transfer rate and radiative decay rate scale with the probability of the donor transition [38,39]. For exchange interaction, the transfer rate is not proportional to the oscillator strengths of the transitions involved on either the donor or acceptor but scales with the overlap of donor and acceptor wave functions [38,41]. There are also situations with no spectral overlap between the emission of donor and the absorption of acceptor where ET can still take place via charge-transfer states, as shown, e.g., in the Ce^{3+}-to-Yb^{3+} case with ET occurring via a Ce^{4+}-Yb^{2+} charge-transfer state

---

*Author to whom correspondence should be addressed:
qyzhang@scut.edu.cn, a.meijerink@uu.nl

T.Y. and D.Y. contributed equally to this work.

(CTS) [36,42,43]. This may also occur for the (Bi^{3+}, Yb^{3+}) couple.

The Bi^{3+} ion possesses a $6s^2$ electronic configuration, giving rise to a ground state $^1S_0$, as well as $^3P_0$, $^3P_1$, $^3P_2$, and $^1P_1$ excited states (in order of increasing energy) [30–32]. The transitions from the ground state $^1S_0$ to the $^3P_0$ or $^3P_2$ levels are spin forbidden, while the transition to $^3P_1$ is partly spin allowed due to admixture of the $^1P_1$ state (as both states have total orbital angular momentum $J = 1$). In view of strong spin-orbit coupling for the heavy Bi^{3+} ion, this mixing can effectively relax the spin selection rule [44–46]. Although the $^3P_0 \rightarrow \, ^1S_0$ transition is forbidden, Bi^{3+} emission from the $^3P_0$ excited state is still observed at low temperature [44,45]. The forbidden character of this emission is evidenced by a long lifetime ($\sim$100 μs) that is two orders of magnitude slower than the fast $^3P_1 \rightarrow \, ^1S_0$ transition (μs) [31,44,45]. This characteristic temperature behavior of the donor (Bi^{3+}) decay gives a possibility to distinguish between ET mechanisms for Bi^{3+} to Yb^{3+} ET. The transfer rate for cooperative ET mechanism is proportional to the oscillator strength of transition on the donor while for exchange interaction it is independent.

The aim of the present work is to shed light on the underlying mechanism of the Bi^{3+}-to-Yb^{3+} ET process in Y_2O_3. We chose Y_2O_3 as a host lattice because Bi^{3+}-doped yttrium oxide ($Y_2O_3 : Bi^{3+}$) is an efficiently luminescing blue/green phosphor [30,47]. Upon codoping with Yb^{3+}, efficient ET from Bi^{3+} to Yb^{3+} has been reported to occur via cooperative ET, making the material promising as strongly absorbing downconverter for solar cell applications [33–35]. Here we find that the Bi^{3+} to Yb^{3+} ET mechanism is not cooperative, but single-step ET via exchange interaction. By quantitative analysis of the Yb^{3+} concentration dependence of the transfer rate, we find that the results are consistent with the single-step mechanism via a Bi^{4+}-Yb^{2+} CTS. Temperature-dependent luminescence and lifetime measurements further demonstrate that ET occurs via exchange interaction. In particular, the temperature-dependent ET efficiency is shown to strongly decrease with increasing temperature (thermally deactivated ET) which is a unique observation that can only be explained by ET via exchange interaction.

II. EXPERIMENTAL

Microcrystalline Y_2O_3 doped with Bi^{3+} and Yb^{3+} was synthesized via the urea-nitrate solution combustion method described in the literature [33]. The Bi^{3+} concentration was kept constant at 1% while the Yb^{3+} concentration varies from 0% to 20% (0%, 1%, 2%, 5%, 10%, and 20%). All percentages of Bi^{3+} and Yb^{3+} are atomic percentage (or mol %) relative to Y^{3+}. First, stoichiometric amounts of Y_2O_3, Yb_2O_3, and Bi_2O_3 were dissolved in the solution of nitric acid and subsequently urea was added (urea/metal ion = 2:1 in mole). The resulting homogeneous precursor solution was placed in an oven preheated at 500 °C to initiate the combustion process. The obtained amorphous solid precursors were thoroughly ground and further annealed at 1000 °C for 4 h in air to complete the formation of crystalline Y_2O_3. The obtained powder was checked for phase purity with x-ray diffraction (XRD). The XRD patterns show all characteristic
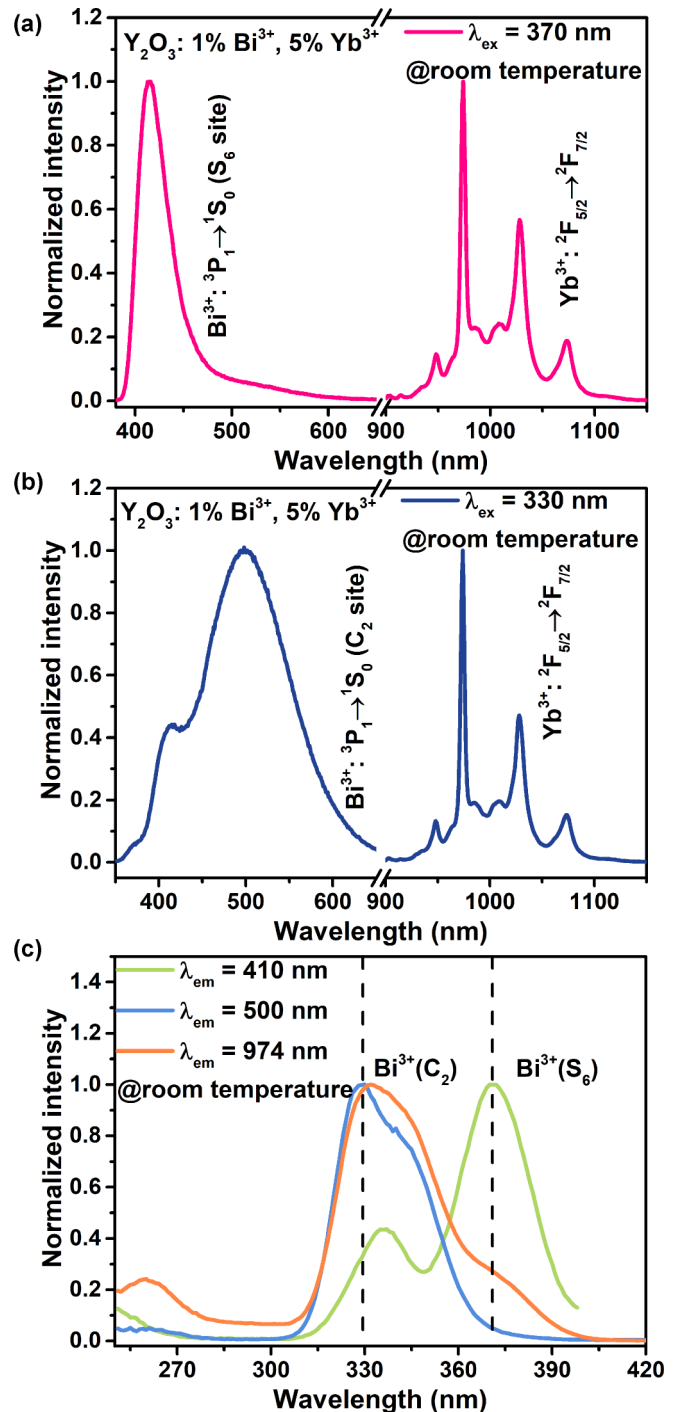

FIG. 1. The normalized visible-NIR emission spectra under excitation (a) at 370 nm, and (b) at 330 nm for Y_2O_3 codoped with 1% Bi^{3+} and 5% Yb^{3+} at room temperature; (c) the normalized excitation spectra monitoring at 410, 500, and 974 nm, respectively, in the same sample.

diffraction peaks for cubic Y_2O_3 and no evidence for the presence of a second crystalline phase.

Emission and excitation spectra were measured using an Edinburgh Instruments FLS920 fluorescence spectrometer with a 450-W xenon lamp as the excitation resource, a 0.3-m excitation double monochromator, and a Hamamatsu R928
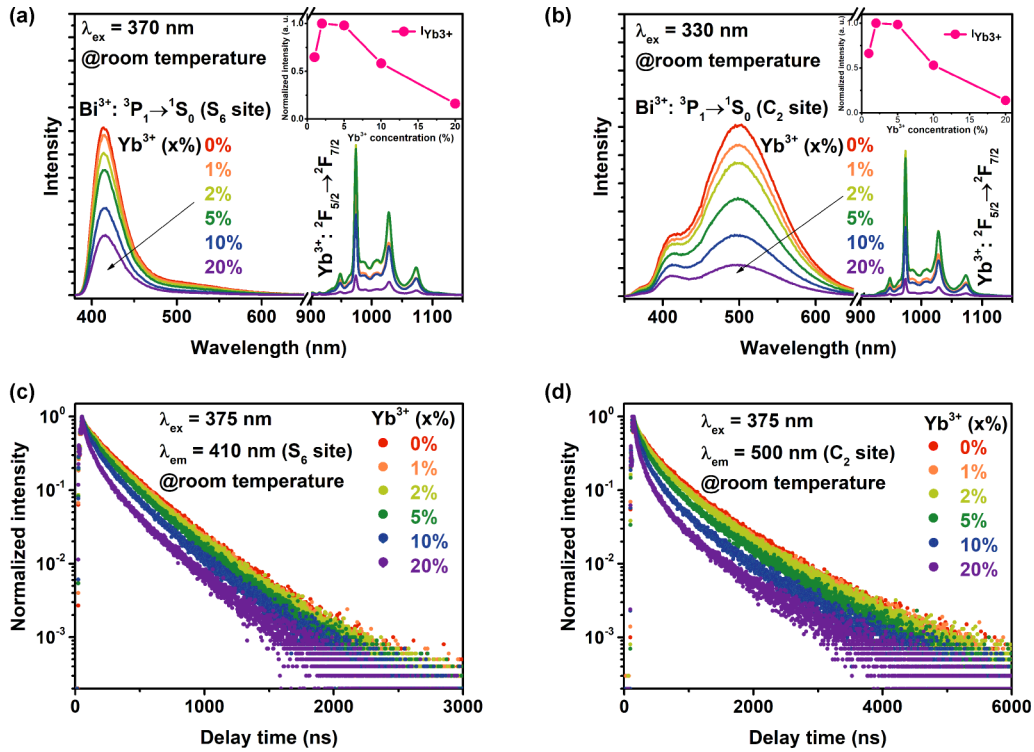
FIG. 2. Visible-NIR spectra of $Y_2O_3 : 1\% Bi^{3+}, x\% Yb^{3+}$ ($x = 0, 1, 2, 5, 10, 20$) under excitation (a) at 370 nm, and (b) at 330 nm at room temperature. Decay curves of the Bi^{3+} emission (c) at 410 nm (S_6 site), and (d) at 500 nm (C_2 site) at room temperature.

photomultiplier tube (PMT) for the 250–800-nm wavelength range or a liquid-nitrogen-cooled Hamamatsu R5509-42 PMT for the 800–1400-nm region. The Edinburgh fluorescence spectrometer is equipped with an Oxford helium flow cryostat for low-temperature measurements. Photoluminescence (PL) decay curves of Bi^{3+} from 100 to 300 K were recorded on the Edinburgh FLS920 system equipped with a fast Hamamatsu H7422-02 PMT using an Edinburgh Instruments EPL375 picosecond pulsed diode laser as excitation source. For decay curves of Bi^{3+} emission from 4 to 75 K, an optical parametric oscillator system (Opotek HE 355 II) pumped by the third harmonic of a Nd:YAG laser (pulse width 10 ns; repetition rate 20 Hz) was used for excitation. The PL decay curves were recorded with a Hamamatsu R928 PMT in combination with the multichannel scaling option available on the Edinburgh Instruments FLS920 fluorescence spectrometer.

III. RESULTS AND DISCUSSION

For $Y_2O_3 : Bi^{3+}$ phosphors the PL properties have been extensively investigated, both experimentally and theoretically [30,31,45,47–50]. In the Y_2O_3 host two types of crystallographic cation sites (Y^{3+}) with symmetry S_6 and C_2 are present in a ratio 1:3. The energy-level structure of Bi^{3+} shows a strong dependence on the local coordination. In the present work, therefore, it is necessary to distinguish the PL behavior of Bi^{3+} ions residing on different sites. Figures 1(a) and 1(b) show the normalized visible-NIR emission spectra of Y_2O_3 codoped with 1% Bi^{3+} and 5% Yb^{3+} under excitation at 370 and 330 nm, respectively. In the visible region, we can see that a narrow emission band centered at 410 nm

[Fig. 1(a)] which is assigned to the $^3P_1 \rightarrow {}^1S_0$ transition of Bi^{3+} on the S_6 site [$Bi^{3+}(S_6)$]. The broad emission band centered at 500 nm ([Fig. 1(b)] is originating from the same transition of Bi^{3+} on the C_2 site [$Bi^{3+}(C_2)$]. These emission spectra are consistent with previous reports [33,45,47,50]. In Fig. 1(b) there is a shoulder at 410 nm, from the emission of $Bi^{3+}(S_6)$ for excitation in the $Bi^{3+}(C_2)$ band at 330 nm. This can be explained by ET between $Bi^{3+}(C_2)$ and $Bi^{3+}(S_6)$. The presence of ET is confirmed by the excitation spectra. In Fig. 1(c), a broad excitation band centered around 330 nm (blue line) is observed and assigned to the $^1S_0 \rightarrow {}^3P_1$ transition of $Bi^{3+}(C_2)$. For the spectrum monitoring $Bi^{3+}(S_6)$ emission at 410 nm (green line), there are two excitation bands at 330 and 370 nm, respectively. The higher excitation band at 370 nm is the typical $^1S_0 \rightarrow {}^3P_1$ transition for $Bi^{3+}(S_6)$ in Y_2O_3 but also a weaker band at 330 nm is observed which coincides with the absorption band of $Bi^{3+}(C_2)$ and provides evidence for ET from $Bi^{3+}(C_2)$ to $Bi^{3+}(S_6)$.

In the NIR region, sharp emission lines between 950 and 1100 nm are observed with the highest intensity peak at 974 nm [Figs. 1(a) and 1(b)]. These emission lines are characteristic of $^2F_{5/2} \rightarrow {}^2F_{7/2}$ emission of Yb^{3+}. When monitoring the Yb^{3+} NIR emission, in the excitation spectrum two broad excitation bands are observed between 310 and 400 nm [Fig. 1(c)]. The positions of the two bands coincide with the $^1S_0 \rightarrow {}^3P_1$ absorption bands of $Bi^{3+}(C_2)$ and $Bi^{3+}(S_6)$. These results indicate that ET does occur from Bi^{3+} (S_6 or C_2 site) to Yb^{3+} in Y_2O_3. The relative intensity of the $Bi^{3+}(C_2)$ excitation band is more than three times stronger than the $Bi^{3+}(S_6)$ excitation bands. A 3:1 ratio would be expected based on a statistical distribution of Bi^{3+} on the

C_2 and S_6 sites. The higher relative intensity of the Bi$^{3+}(C_2)$ excitation band suggests that the Bi$^{3+}(C_2)$ to Yb^{3+} ET is more efficient than Bi$^{3+}(S_6)$-Yb^{3+}ET. Alternatively, there may be a preference for Bi^{3+} to substitute on the Y$^{3+}(C_2)$ site. At shorter wavelengths, around 260 nm, an additional weak band is observed in the excitation spectrum of the Yb^{3+} 974-nm emission. This could be a tail of the Yb^{3+} charge-transfer band or a defect absorption directly feeding the $^2F_{5/2}$ level of Yb^{3+}.

To investigate the influence of Yb^{3+} content on the Bi^{3+}-to-Yb^{3+} ET, we measured visible-NIR emission spectra and decay curves for Y$_2$O$_3$: 1% Bi^{3+} codoped with 0%, 1%, 2%, 5%, 10%, and 20% Yb^{3+}. Figure 2(a) shows emission spectra under excitation at 370 nm. With increasing Yb^{3+} concentration, the Bi$^{3+}(S_6)$ emission intensity decreases and the Yb^{3+} emission intensity increases to reach a maximum at 2% Yb^{3+} content and then decreases [see inset in Fig. 2(a)]. The decrease is explained by concentration quenching. As the Yb^{3+} concentration increases beyond 2% energy migration among Yb^{3+} ions occurs to impurities and defects, i.e., OH$^-$ groups. Upon excitation at 330 nm even more pronounced PL quenching is observed for Bi$^{3+}(C_2)$ emission [Fig. 2(b)]. It is evident that ET from Bi^{3+} to Yb^{3+} is very efficient, even at low Yb^{3+} concentrations. This is not expected for cooperative ET which is a second-order process involving simultaneous transfer to two Yb^{3+} ions in close proximity to the Bi^{3+} donor. Typically, cooperative ET becomes efficient at high acceptor concentrations.

A powerful method to extract quantitative information on dynamics and mechanism of ET processes is analysis of luminescence decay curves. Figures 2(c) and 2(d) show the room-temperature luminescence decay curves for the Bi$^{3+}(S_6)$ emission at 410 nm and for the Bi$^{3+}(C_2)$ emission at 500 nm, respectively. The decay becomes faster and more nonexponential as the Yb^{3+} content increases. Due to the nonexponential character of decay curves, the average lifetime τ_{avr} of the Bi^{3+} excited state was determined by

$$\tau_{avr} = \frac{\int I(t)t\,dt}{\int I(t)\,dt}, \qquad (1)$$

where $I(t)$ is the emission intensity at a time t after the excitation pulse. For the Bi$^{3+}(S_6)$ emission the lifetime is reduced from 204 ns for the singly doped Bi^{3+} material to 100 ns for Y$_2$O$_3$ codoped with 20% Yb^{3+}. For the Bi$^{3+}(C_2)$ emission the lifetime drops from 336 to 131 ns with Yb^{3+} content varying from 0% to 20%. This shows that ET to Yb^{3+} is efficient. The efficiency of ET η_{ET} can be estimated as

$$\eta_{ET} = \left(1 - \frac{\tau_{avr}^{x\%Yb}}{\tau_{avr}^{0\%Yb}} \right) \times 100\%, \qquad (2)$$

where the superscript $x\%$Yb is the concentration of Yb^{3+} in samples. For Bi^{3+} on the S_6 site the transfer efficiency is 51% for Y$_2$O$_3$: 1% Bi^{3+}, 20% Yb^{3+}, whereas a transfer efficiency of 61% is obtained for Bi$^{3+}(C_2)$-to-Yb^{3+}ET. This is consistent with the faster decrease of Bi^{3+} emission behavior in Fig. 2(b).

The results above confirm the occurrence of efficient ET between Bi^{3+} and Yb^{3+} in Y$_2$O$_3$. However, the ET mechanism cannot be established although the efficient ET observed for relatively low Yb^{3+} concentrations indicates that
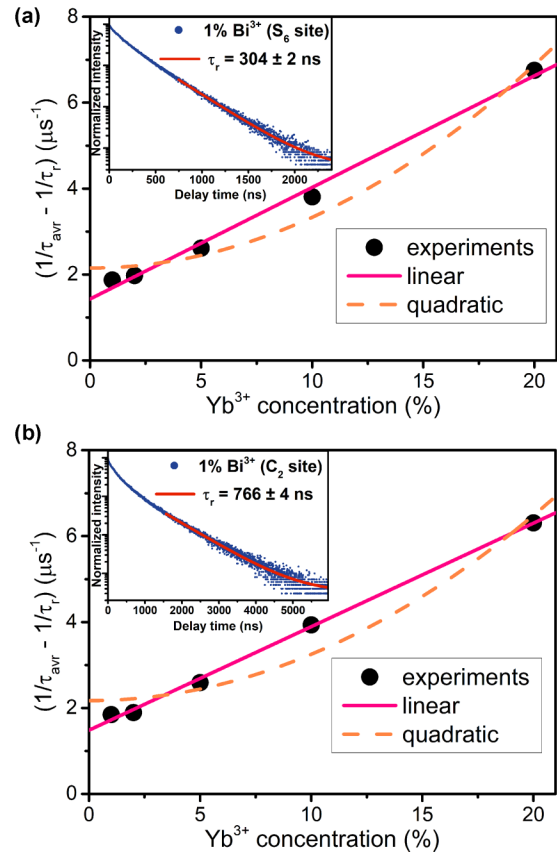

FIG. 3. The Yb^{3+}-concentration dependence of $\frac{1}{\tau_{avr}} - \frac{1}{\tau_r}$ for (a) Bi$^{3+}(S_6)$ emission, and for (b) Bi$^{3+}(C_2)$ emission. The solid line (magenta) shows a linear fit and the dashed curve (orange) represents a quadratic fit. Inset shows the decay curves of Bi^{3+} emission (a) in the S_6 site and (b) in the C_2 site with a single-exponential fit in the long-time regime.

the mechanism is not cooperative ET as previously suggested in the literature [21]. To obtain further insight into the ET mechanism, we analyzed the average rate of ET between Bi^{3+} (on S_6 or C_2 site) and neighboring Yb^{3+} ions as a function of Yb^{3+} content. The decay curves for the Bi^{3+} emission in the singly doped (1% Bi^{3+}) Y$_2$O$_3$ are nonexponential. This implies that in addition to radiative decay other deexcitation processes are active, e.g., ET between Bi^{3+} ions and/or ET to quenching center. In the long-time regime, the tail of the curve becomes single exponential with a decay time corresponding to the radiative lifetime, τ_r [see inset of Figs. 3(a) and 3(b)]. The values are in good agreement with results for Y$_2$O$_3$ with lower Bi^{3+} concentration (0.5%) [31]. Upon codoping with Yb^{3+}, ET is an additional decay channel. The average ET rate can be obtained by the following expression:

$$W_{ET} + W_0 = \frac{1}{\tau_{avr}} - \frac{1}{\tau_r}, \qquad (3)$$

where W_{ET} is the average ET rate of Bi^{3+} to Yb^{3+} and W_0 represents the rate of other nonradiative decay processes of Bi^{3+}. Figure 3(a) shows the Yb^{3+}-concentration dependence of $\frac{1}{\tau_{avr}} - \frac{1}{\tau_r}$ for Bi$^{3+}(S_6)$ emission. Both visual inspection and comparison of fits to a linear or quadratic function show that the linear dependence matches the experimental results better.
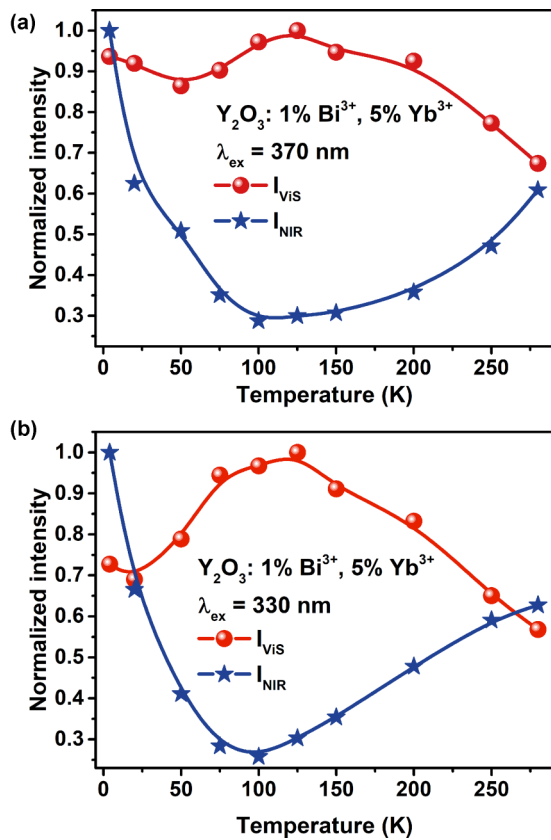
FIG. 4. Temperature dependence of the normalized integrated intensities of the Bi^{3+} emission and the Yb^{3+} emission for Y_2O_3 codoped with 1% Bi^{3+} and 5% Yb^{3+} under excitation (a) at 370 nm and (b) at 330 nm.

This shows that Bi^{3+}-to-Yb^{3+} ET does not fit cooperative ET (giving a quadratic concentration dependence) and points toward a one-to-one photon conversion process. A similar dependence is observed for $Bi^{3+}(C_2)$ emission [Fig. 3(b)].

To gain insight into the ET mechanism, temperature-dependent luminescence and lifetime measurements were performed. Figure 4(a) shows the temperature dependence of the normalized integrated intensity of Bi^{3+} emission and that of Yb^{3+} emission in Y_2O_3 codoped with 1% Bi^{3+} and 5% Yb^{3+} under excitation at 370 nm. The temperature dependence is unusual: Upon raising the temperature from 4 to $\sim$100 K the relative emission intensity of the Bi^{3+} donor increases while the emission intensity of Yb^{3+} acceptor decreases. This behavior is opposite from the more commonly observed thermally activated ET and demonstrates that the ET efficiency is thermally deactivated between 4 and 100 K. In Fig. 4(b) the normalized intensities for the Bi^{3+} emission and Yb^{3+} emission are shown for excitation at 330 nm. A similar trend is observed with a strong decrease of the Yb^{3+} emission between 4 and 100 K. Above 100 K the intensity of the Bi^{3+} emission decreases again while the Yb^{3+} emission intensity increases. This indicates that above 100 K the usually observed thermally activated energy transfer is operative. For singly Bi-doped Y_2O_3 a similar temperature-dependent behavior of the Bi^{3+} emission was reported [45].

To understand this peculiar temperature dependence, luminescence decay curves were measured both for singly doped Y_2O_3 : 1% Bi^{3+} and codoped material with 5% or 20% Yb^{3+}. In Fig. 5 the decay curves of the $Bi^{3+}(S_6)$ emission are shown for six temperatures (4, 50, 100, 150, 200, and 250 K). The violet curves show the decay of the Bi^{3+} emission in the singly doped (1% Bi^{3+}) Y_2O_3, the orange curves for 5% codoping
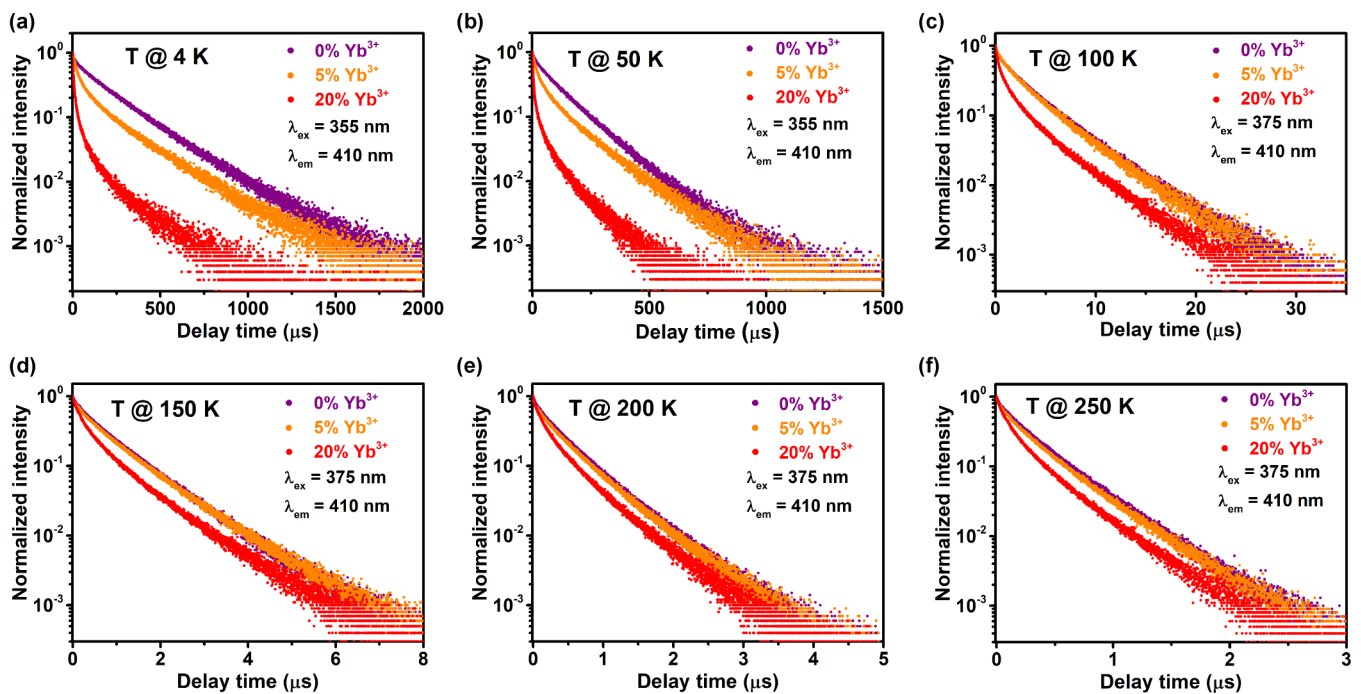

FIG. 5. Decay curves of the Bi^{3+} emission at 410 nm for Y_2O_3 : 1% Bi^{3+} codoped with 0%, 5%, 20% Yb^{3+}, taken at the temperatures (a) 4 K, (b) 50 K, (c) 100 K, (d) 150 K, (e) 200 K, and (f) 250 K.
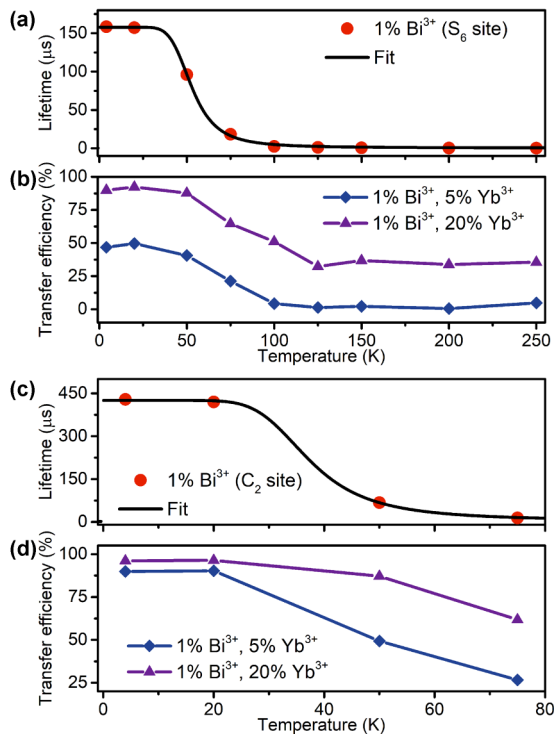
FIG. 6. Temperature-dependent lifetimes of the Bi^{3+} luminescence of $Y_2O_3 : 1\% Bi^{3+}$ when Bi^{3+} occupies S_6 site (a) and Bi^{3+} occupies C_2 site (c), as well as temperature dependence of the transfer efficiency of $Bi^{3+}(S_6)$-to-Yb^{3+} (b) and that of $Bi^{3+}(C_2)$-to-Yb^{3+} (d) in $Y_2O_3 : 1\% Bi^{3+}$ codoped with 5% and 20% Yb^{3+}. Note the black line represents a three-level fit.

with Yb^{3+}, and the red curves for 20% Yb^{3+} codoping. Note the large change in timescales along the x axes from 2000 μs at 4 K to 3 μs at 300 K. In Figs. 6(a) and 6(c) the temperature dependence of the decay times of the Bi^{3+} emission for $Bi^{3+}(S_6)$ and $Bi^{3+}(C_2)$ are shown.

The change in decay time for the Bi^{3+} emission follows the typical behavior of an s^2 ion. The Bi^{3+} ground state is $6s^2$ while the excited state is $6s6p$. The $6s6p$ excited state splits in a higher-energy $^1P_1$ and lower-energy ^3P_J states. The ^3P excited state is split by spin-orbit coupling into a $^3P_0$, $^3P_1$, and $^3P_2$ state. The transition from the lowest-energy $^3P_0$ state to the $^1S_0$ ground state is spin forbidden and has a typical decay time of hundreds of μs. Emission from the higher-energy $^3P_1$ level is spin enabled by admixture of the higher-energy $^1P_1$ state (J mixing) and has a typical decay time of a few μs. Upon raising the temperature thermal population of the $^3P_1$ level gives a characteristic shortening of the radiative lifetime. The energy separation between the $^3P_0$ and $^3P_1$ levels varies but is typically between 50 and 1000 cm^{-1} [31,44,45]. Thermal population of the $^3P_1$ level gives rise to sharp decrease in the decay time around temperatures varying between 20 and 150 K. This characteristic behavior is clearly observed in Figs. 6(a) and 6(c). With increasing temperature, the average lifetime decreases sharply from 159 μs ($T = 4$ K) to 2.5 μs ($T = 100$ K) for $Bi^{3+}(S_6)$ and from 428 μs ($T = 4$ K) to 14.2 μs ($T = 75$ K) for $Bi^{3+}(C_2)$. These results are in agreement with the literature reported by van de Craats and Blasse [45]. A three-level fit for the temperature-dependent lifetimes of the

Bi^{3+} emission gives a good description of the experimental data [drawn lines in Figs. 6(a) and 6(c)] and yields an intrinsic lifetime of the $^3P_0 \rightarrow {}^1S_0$ transition (τ_0), 158 and 426 μs, and energy differences between $^3P_1$ and $^3P_0$ (ΔE) of 270 and 161 cm^{-1}, for $Bi^{3+}(S_6)$ and $Bi^{3+}(C_2)$, respectively, in agreement with values found in Ref. [45].

In the same temperature regime where the radiative decay rate of the $^3P_{0,1} \rightarrow {}^1S_0$ emission of Bi^{3+} increases, the ET efficiency strongly decreases as is evidenced by a drop in the Yb^{3+} emission intensity between 4 and 100 K (Fig. 4). This can be understood if the ET mechanism is exchange interaction. For ET via exchange, the excitation energy is transferred by electron exchange between donor and acceptor. This mechanism is fundamentally different from ET via dipole-dipole interaction where interaction strength is governed by the dipole strengths (transition dipole moments) of resonant (electric dipole) transitions on the donor and acceptor and of course by the donor-acceptor distance. For exchange interaction wave-function overlap of occupied and unoccupied wave functions on the donor and acceptor govern the ET probability. Since wave-function overlap decreases exponentially with distance, exchange interaction is short range and typically only observed between nearest neighbors. If the Bi^{3+} to Yb^{3+} ET proceeds via exchange interaction, the rapid increase in radiative decay of the Bi^{3+} (due to the increase in dipole strength by thermal population of the $^3P_1$ level) will not affect the ET rate for ET via exchange interaction. As a result, the radiative decay rate increases and will become faster than the constant ET rate, which explains the rapid decrease in ET efficiency. This is only observed for ET via exchange interaction. For dipole-dipole interaction the ET rate scales with the oscillator strength of the donor transition and the increase in radiative decay rate is accompanied by the same increase in ET rate, making the ET efficiency independent of the oscillator strength of the donor transition.

The luminescence decay curves can also be used to demonstrate and quantify the decrease in ET efficiency with increasing temperatures between 4 and 100 K. The luminescence decay curves in Fig. 5 show at 4 K a significant change in decay behavior upon codoping with 5% or 20% Yb^{3+}. A much faster decay is observed because of ET to Yb^{3+}. As the temperature is raised the $^3P_{0,1} \rightarrow {}^1S_0$ of Bi^{3+} radiative decay becomes faster (violet decay curves) and the change in decay behavior after codoping with 5% (orange curves) or 20% (red curves) of Yb^{3+} is strongly reduced. This is consistent with the discussion above and confirms that as the Bi^{3+} radiative decay rate strongly increases with temperature, the ET rate does not. Using Eqs. (1) and (2), the average lifetime and ET efficiencies can be determined from the experimental decay curves. The ET efficiency as a function of temperature is shown in Figs. 6(b) and 6(d) for Bi^{3+} on the S_6 site and the C_2 site, respectively. The efficiency of $Bi^{3+}(S_6)$-Yb^{3+} decreases from 47% ($T = 4$ K) to 4% ($T = 100$ K), and from 90% ($T = 4$ K) to 32% ($T = 100$ K) in $Y_2O_3 : 1\% Bi^{3+}$ with 5% and 20% Yb^{3+}, respectively. With increasing temperature, a similar rapid decrease of efficiency of $Bi^{3+}(C_2)$ is observed from 90% at 4 K to 26% at 75 K, from 96% at 4 K to 61% at 75 K, for $Y_2O_3 : 1\% Bi^{3+}$ codoped with 5% and 20% Yb^{3+}, respectively. The unusual observation of thermally deactivated ET provides convincing evidence that the ET mechanism is exchange interaction. The

analysis of the temperature-dependent emission spectra and decay curves of Y_2O_3 codoped with Bi^{3+} and Yb^{3+} clearly demonstrates that the mechanism of Bi^{3+}-to-Yb^{3+} ET is not cooperative downconversion, but is through a single-step ET via exchange interaction. For cooperative ET, the transfer rate W_{ET} is proportional to the decay rate of the excited state of the donor, and thus the ET efficiency is independent of the lifetime of the donor emission, which is in inconsistent with the results in Figs. 6(b) and 6(d).

ET via exchange interaction can occur via the Bi^{4+}-Yb^{2+} charge-transfer state similar to the Ce^{3+}-to-Yb^{3+} ET via a Ce^{4+}-Yb^{2+} CTS. This is consistent with recent work by Awater and Dorenbos [46], who constructed the vacuum referred binding energy to describe the location of levels of $Ln^{3+}/^{2+}$ and Bi^{3+}. The diagram (see Fig. 11 in Ref. [46]) shows the $^3P_{0,1}$ level of Bi^{3+} is about 0.2 eV higher in energy than that of the Yb^{2+} ground state in Y_2O_3, indicating that charge transfer is favorable from Bi^{3+} excited state to form a Bi^{4+}-Yb^{2+} CTS. Hence, we conclude that the ET mechanism between Bi^{3+} and Yb^{3+} in Y_2O_3 is a single-step ET process via Bi^{4+}-Yb^{2+} CTS. It is interesting to investigate if this ET mechanism is also operative in other host materials codoped with Bi^{3+} and Yb^{3+}. Presently, work is ongoing to investigate this.

IV. CONCLUSIONS

In this paper, the ET between Bi^{3+} and Yb^{3+} in Y_2O_3 has been investigated using steady-state and time-resolved luminescence spectroscopy between 4 and 300 K. The Yb^{3+}-concentration dependence of the ET efficiency indicates that Bi^{3+}-to-Yb^{3+} ET occurs through a single-step ET mechanism and not via cooperative ET as reported in the literature. Temperature-dependent measurements reveal an unexpected drop in ET efficiency upon raising the temperature from 4 to 100 K. This unusual observation of thermally deactivated ET can be understood if Bi^{3+}-to-Yb^{3+} ET occurs via exchange interaction. The rate for ET via exchange interaction is independent of the oscillator strength of donor and acceptor. This constant ET rate leads to a lower ET efficiency in the temperature regime where thermal population of the $^3P_1$ level of Bi^{3+} gives rise to a faster donor emission decay rate. The results demonstrate that UV-to-NIR conversion in Y_2O_3 : Bi^{3+}, Yb^{3+} involves single-step ET probably via a Bi^{4+}-Yb^{2+} charge-transfer state and warrants further research into the ET mechanism for other host materials for which photon splitting by cooperative ET from Bi^{3+} to Yb^{3+} has been reported.

[1] D. L. Dexter, Phys. Rev. **108**, 630 (1957).

[2] R. T. Wegh, H. Donker, K. D. Oskam, and A. Meijerink, Science **283**, 663 (1999).

[3] T. Trupke, M. A. Green, and P. Würfel, J. Appl. Phys. **92**, 1668 (2002).

[4] B. S. Richards, Sol. Energy Mater. Sol. Cells **90**, 1189 (2006).

[5] Z. R. Abrams, A. Niv, and X. Zhang, J. Appl. Phys. **109**, 114905 (2011).

[6] A. Boccolini, J. Marques-Hueso, D. Chen, Y. Wang, and B. S. Richards, Sol. Energy Mater. Sol. Cells **122**, 8 (2014).

[7] L. Wondraczek, E. Tyystjärvi, J. Méndez-Ramos, F. A. Müller, and Q. Zhang, Adv. Sci. **2**, 1500218 (2015).

[8] M. B. de la Mora, O. Amelines-Sarria, B. M. Monroy, C. D. Hernández-Pérez, and J. E. Lugo, Sol. Energy Mater. Sol. Cells **165**, 59 (2017).

[9] Q. Y. Zhang and X. Y. Huang, Prog. Mater. Sci. **55**, 353 (2010).

[10] C. Lorbeer and A.-V. Mudring, Chem. Commun. **50**, 13282 (2014).

[11] P. Ghosh and A. V. Mudring, Nanoscale **8**, 8160 (2016).

[12] M. de Jong, A. Meijerink, and F. T. Rabouw, Nat. Commun. **8**, 15537 (2017).

[13] W. Shao, G. Chen, T. Y. Ohulchanskyy, C. Yang, H. Ågren, and P. N. Prasad, Nanoscale **9**, 1934 (2017).

[14] D. C. Yu, S. Ye, M. Y. Peng, Q. Y. Zhang, and L. Wondraczek, Appl. Phys. Lett. **100**, 191911 (2012).

[15] D. Serrano, A. Braud, J. L. Doualan, W. Bolaños, R. Moncorgé, and P. Camy, Phys. Rev. B **88**, 205144 (2013).

[16] D.-C. Yu, R. Martín-Rodríguez, Q.-Y. Zhang, A. Meijerink, and F. T. Rabouw, Light: Sci. Appl. **4**, e344 (2015).

[17] B. Zhou, L. Tao, Y. Chai, S. P. Lau, Q. Zhang, and Y. H. Tsang, Angew. Chem. Int. Ed. **128**, 12544 (2016).

[18] Y.-T. An, C. Labbé, J. Cardin, M. Morales, and F. Gourbilleau, Adv. Opt. Mater. **1**, 855 (2013).

[19] L. Dumont, J. Cardin, P. Benzo, M. Carrada, C. Labbé, A. L. Richard, D. C. Ingram, W. M. Jadwisienczak, and F. Gourbilleau, Sol. Energy Mater. Sol. Cells **145**, 84 (2016).

[20] L. Zhou, P. A. Tanner, W. Zhou, Y. Ai, L. Ning, M. M. Wu, and H. Liang, Angew. Chem. Int. Ed. **56**, 10357 (2017).

[21] P. Vergeer, T. J. H. Vlugt, M. H. F. Kox, M. I. den Hertog, J. P. J. M. van der Eerden, and A. Meijerink, Phys. Rev. B **71**, 014119 (2005).

[22] Q. Y. Zhang, G. F. Yang, and Z. H. Jiang, Appl. Phys. Lett. **91**, 051903 (2007).

[23] S. Ye, B. Zhu, J. Chen, J. Luo, and J. R. Qiu, Appl. Phys. Lett. **92**, 141112 (2008).

[24] D. Chen, Y. Yu, Y. Wang, P. Huang, and F. Weng, J. Phys. Chem. C **113**, 6406 (2009).

[25] J.-M. Meijer, L. Aarts, B. M. van der Ende, T. J. H. Vlugt, and A. Meijerink, Phys. Rev. B **81**, 035107 (2010).

[26] J. T. van Wijngaarden, S. Scheidelaar, T. J. H. Vlugt, M. F. Reid, and A. Meijerink, Phys. Rev. B **81**, 155112 (2010).

[27] W. Zheng, H. Zhu, R. Li, D. Tu, Y. Liu, W. Luo, and X. Chen, Phys. Chem. Chem. Phys. **14**, 6974 (2012).

[28] T. Yu, D. C. Yu, H. H. Lin, and Q. Y. Zhang, J. Alloys Compd. **695**, 1154 (2017).

[29] T. Sun, X. Chen, L. Jin, H. W. Li, B. Chen, B. Fan, B. Moine, X. Qiao, X. Fan, S. W. Tsang, S. F. Yu, and F. Wang, J. Phys. Chem. Lett. **8**, 5099 (2017).

[30] G. Blasse and A. Bril, J. Chem. Phys. **48**, 217 (1968).

[31] G. Boulon, J. Phys. (Paris) **32**, 333 (1971).

[32] R. Moncorgé and G. Boulon, J. Lumin. **18**, 376 (1979).

[33] X. Y. Huang, X. H. Ji, and Q. Y. Zhang, J. Am. Ceram. Soc. **94**, 833 (2011).

[34] G. Gao, M. Peng, and L. Wondraczek, J. Mater. Chem. C **2**, 8083 (2014).

[35] Y. Zhydachevskyy, V. Tsiumra, M. Baran, L. Lipińska, P. Sybilski, and A. Suchocki, J. Lumin. **196**, 169 (2018).

[36] D. C. Yu, F. T. Rabouw, W. Q. Boon, T. Kieboom, S. Ye, Q. Y. Zhang, and A. Meijerink, Phys. Rev. B **90**, 165126 (2014).

[37] F. T. Rabouw and A. Meijerink, J. Phys. Chem. C **119**, 2364 (2015).

[38] D. L. Dexter, J. Chem. Phys. **21**, 836 (1953).

[39] K. B. Eisenthal and S. Siegel, J. Chem. Phys. **41**, 652 (1964).

[40] F. T. Rabouw, S. A. den Hartog, T. Senden, and A. Meijerink, Nat. Commun. **5**, 3610 (2014).

[41] M. Inokuti and F. Hirayama, J. Chem. Phys. **43**, 1978 (1965).

[42] J. Ueda and S. Tanabe, J. Appl. Phys. **106**, 043101 (2009).

[43] A. D. Sontakke, J. Ueda, Y. Katayama, P. Dorenbos, and S. Tanabe, Appl. Phys. Lett. **106**, 131906 (2015).

[44] G. Boulon, C. K. Jørgensen, and R. Reisfeld, Chem. Phys. Lett. **75**, 24 (1980).

[45] A. van de Craats and G. Blasse, Chem. Phys. Lett. **243**, 559 (1995).

[46] R. H. P. Awater and P. Dorenbos, J. Lumin. **184**, 221 (2017).

[47] L. G. Jacobsohn, M. W. Blair, S. C. Tornga, L. O. Brown, B. L. Bennett, and R. E. Muenchausen, J. Appl. Phys. **104**, 124303 (2008).

[48] H. Choi, S. H. Cho, S. Khan, K.-R. Lee, and S. Kim, J. Mater. Chem. C **2**, 6017 (2014).

[49] F. Réal, V. Vallet, J.-P. Flament, and J. Schamps, J. Chem. Phys. **127**, 104705 (2007).

[50] V. Babin, K. Chernenko, L. Lipińska, E. Mihokova, M. Nikl, L. S. Schulman, T. Shalapska, A. Suchocki, S. Zazubovich, and Y. Zhydachevskii, J. Lumin. **167**, 268 (2015).